AGU ADVANCING EARTH AND SPACE SCIENCES

Geophysical Research Letters

RESEARCH LETTER
10.1029/2025GL116714

The Remarkable 2024 North Atlantic Mid-Season Hurricane Lull

P. J. Klotzbach[1], E. Bercos-Hickey[2], K. M. Wood[3], C. J. Schreck III[4], M. M. Bell[1], E. S. Blake[5], S. G. Bowen[6], L.-P. Caron[7], D. R. Chavas[8], J. M. Collins[9], E. J. Gibney[10†], K. A. Hansen[11], A. T. Hazelton[12], J. J. Jones[13], M. R. Lowry[14], A. T. Nieves-Jimenez[1], C. M. Patricola[2,15], L. G. Silvers[1], R. E. Truchelut[16], and J. Uehling[4]

[1]Department of Atmospheric Science, Colorado State University, Fort Collins, CO, USA, [2]Climate and Ecosystem Sciences Division, Lawrence Berkeley National Laboratory, Berkeley, CA, USA, [3]Department of Hydrology and Atmospheric Sciences, The University of Arizona, Tucson, AZ, USA, [4]North Carolina Institute for Climate Studies, Cooperative Institute for Satellite Earth Systems Studies, North Carolina State University, Asheville, NC, USA, [5]NOAA/National Hurricane Center, Miami, FL, USA, [6]Gallagher Re, Chicago, IL, USA, [7]Ouranos, Montreal, QC, Canada, [8]Department of Earth, Atmospheric and Planetary Sciences, Purdue University, West Lafayette, IN, USA, [9]School of Geosciences, University of South Florida, Tampa, FL, USA, [10]University Corporation for Atmospheric Research/Cooperative Programs for the Advancement of Earth System Science, San Diego, CA, USA, [11]National Research Council, Washington, DC, USA, [12]University of Miami CIMAS/NOAA AOML, Miami, FL, USA, [13]Department of Physics, University of the West Indies, Kingston, Jamaica, [14]WPLG TV, Miami, FL, USA, [15]Department of the Earth, Atmosphere, and Climate, Iowa State University, Ames, IA, USA, [16]WeatherTiger LLC, Tallahassee, FL, USA

†Deceased

Key Points:

- Following an active start, the 2024 Atlantic hurricane was quiet during the climatological peak with only 1 tropical storm and 1 hurricane
- The lull was not anticipated by seasonal forecasting agencies, which called for an extremely active 2024 Atlantic hurricane season
- Factors reducing storm count included a northward shift in African easterly waves, broad-scale subsidence, and reduced mid-level moisture

Supporting Information:

Supporting Information may be found in the online version of this article.

Correspondence to:

P. J. Klotzbach,
philk@atmos.colostate.edu

Citation:

Klotzbach, P. J., Bercos-Hickey, E., Wood, K. M., Schreck, C. J., III, Bell, M. M., Blake, E. S., et al. (2025). The remarkable 2024 North Atlantic mid-season hurricane lull. *Geophysical Research Letters*, *52*, e2025GL116714. https://doi.org/10.1029/2025GL116714

Received 25 APR 2025
Accepted 15 SEP 2025

Abstract

The 2024 North Atlantic (hereafter Atlantic) hurricane season started quickly, with the earliest Category 5 on record (Beryl) and three hurricanes forming through 14 August. Following Ernesto's dissipation on 20 August, the Atlantic hurricane season became extremely quiet during the climatological peak of hurricane season, with only one Category 2 hurricane (Francine) and one tropical storm through 23 September. Several environmental factors likely contributed to this unexpected, prolonged lull. During mid-to-late August, subseasonal conditions were broadly favorable for Atlantic hurricanes, but a northward shift in African easterly wave emergence latitude yielded fewer tropical cyclone seed disturbances that also traversed unfavorably cool ocean water. During early-to-mid September, subseasonal variability driven by the Madden-Julian oscillation was less conducive to hurricane activity, with several bouts of increased vertical wind shear across the central Atlantic. Throughout most of the lull, the tropical Atlantic was anomalously dry and subsident, suppressing hurricane formation chances.

Plain Language Summary

The 2024 North Atlantic (hereafter Atlantic) hurricane season was anticipated to be extremely active, with seasonal forecasts calling for a potentially historic season. Following a busy start including the earliest Category 5 Atlantic hurricane on record (Beryl), the season became very quiet between 20 August–23 September, with only one Category 2 hurricane (Francine) and one tropical storm forming. Following the lull, the Atlantic became extremely busy again, with seven hurricanes forming from 25 September through the end of the season–the most on record for this period. This paper focuses on the surprising lull and attributes it to several different factors, including a late-August northward shift in African easterly wave tracks (organized thunderstorm complexes spanning thousands of kilometers that often serve as Atlantic hurricane seeds). This northward shift brought these systems out over colder water and into a drier airmass, suppressing their hurricane formation chances. During the first 3 weeks of September, a large-scale tropical phenomenon known as the Madden-Julian oscillation, resulted in increased sinking motion, drier mid-levels and increased vertical wind shear–all of which typically reduce Atlantic hurricane activity. Overall, the lull demonstrates how seed disturbances and other environmental factors can strongly modulate aggregate seasonal tropical cyclone activity.

1. Introduction

The 2024 North Atlantic (hereafter Atlantic) hurricane season was predicted to be extremely active, with most seasonal hurricane forecasts calling for one of the most active seasons on record. The average Atlantic hurricane forecast during May–June 2024 from the Seasonal Hurricane Predictions platform https://seasonalhurricanepredictions.org/) called for ~11 hurricanes and 214 × 10^4 kt^2 Accumulated Cyclone Energy (ACE;

Bell et al., 2000). The average Atlantic hurricane season, based on the National Oceanic and Atmospheric Administration's (NOAA) current 30-year climatology of 1991–2020, has 7 hurricanes and 123 ACE. Three reasons frequently given for the hyperactive (>159.6 ACE per NOAA's definition) seasonal forecasts issued in late May/early June were the highest May sea surface temperatures (SSTs) in the Main Development Region (MDR; defined to be 10°–20°N, 85°–20°W in this paper) on record (since 1940), an anticipated shift toward neutral El Niño-Southern Oscillation (ENSO) or La Niña conditions, as well as an anticipated TC-conducive West African monsoon (e.g., increased precipitation, increased low-level horizontal vorticity and a northward-shifted African easterly jet). All of these conditions have been shown to favor active Atlantic hurricane seasons by creating a more favorable thermodynamic and dynamic environment for hurricanes, including increases in mid-level moisture and decreases in vertical wind shear (e.g., Gray, 1984; Klotzbach et al., 2022; Landsea & Gray, 1992; Patricola et al., 2014).

Accordingly, the 2024 Atlantic hurricane season got off to an early start, including the earliest calendar year Category 5 hurricane on record (Beryl). While the Atlantic hurricane data set (HURDAT2; Landsea & Franklin, 2013) extends back to 1851, reliable data for the records noted in this manuscript likely extend back to the early 1970s due to satellite coverage, consistent use of the Dvorak technique and limited aircraft reconnaissance penetrations of strong hurricanes with small eyes prior to the early 1970s (e.g., Delgado et al., 2018; Hagen & Landsea, 2012). Above-average activity continued through the middle of August, with Hurricanes Debby and Ernesto forming by 14 August. On average, only one hurricane has formed in the Atlantic by 14 August.

Following Ernesto's dissipation on 20 August, Atlantic tropical cyclone (TC) activity markedly decreased, with only one Category 2 hurricane (Francine) and one tropical storm (Gordon) forming during the climatological peak of the season between 20 August–23 September. On average, ∼54% of the total seasonal ACE occurs between these two dates, but in 2024 this period only generated ∼7 ACE, which was ∼5% of the total seasonal ACE generated during the season (Figure S1 in Supporting Information S1). This total is the least produced between these two dates since 1994 (∼6 ACE) and the lowest since the beginning of the recent active Atlantic hurricane era (1995–onwards; e.g., Keim et al., 2024). In addition, the one hurricane that formed between 20 August–23 September in 2024 was the lowest during this period since 2009. On average, three hurricanes form between these two dates.

This lull occurred even though MDR-averaged SSTs were the second highest on record during the month of September (∼1.0°C greater than the 1991–2020 average). By comparison, between 20 August–23 September in 2023, with similarly high SSTs over the MDR, the Atlantic generated ∼102 ACE despite strong El Niño conditions that typically suppress Atlantic hurricane activity (e.g., Gray, 1984). MDR-averaged SSTs were also ∼0.3°C warmer during September in 2024 than in 2010, which was the third warmest Atlantic MDR recorded. The 2010 season recorded 12 hurricanes.

Beginning with Helene's formation on 24 September, the Atlantic became extremely active, with 11 named storms, 7 hurricanes, and 4 major (Category 3+; maximum sustained winds ≥96 kt) hurricanes forming during the remainder of the season. The late season was one of the most active on record for the Atlantic and set the record for the most hurricane formations from 25 September onwards. Overall, the season ended up being classified as hyperactive, with a total of 18 named storms, 11 hurricanes, 5 major hurricanes, and ∼162 ACE. This late-season burst of ACE which allowed the season to reach hyperactive levels was especially impressive given that the climatological peak of the season was so quiet.

Though the busy end to the season warrants its own study, this paper focuses on the period between 20 August and 23 September and proposes several likely drivers of the unexpected lull: a northward-shift in African easterly wave (AEW) tracks, increased atmospheric stability due to anomalously warm upper-levels (and associated decreases in potential intensity), increased subsidence and occasional increases in shear driven by convectively-suppressed phases of the Madden-Julian oscillation (MJO), as well as dry air advection from the mid-latitudes.

2. Data and Methods

2.1. Tropical Cyclone Data

All TC data are taken from the Atlantic hurricane best track (HURDAT2; Landsea & Franklin, 2013). This data set spans 1851–2024 at predominately six-hourly time intervals (although interim time periods are available for

specific events such as landfalls and notable intensity changes) and is the best estimate of a storm's characteristics including latitude, longitude, maximum sustained wind, minimum sea level pressure, and various TC structural characteristics.

2.2. Atmosphere-Ocean Environmental Parameter Data

We use the 31-km fifth generation of the European Centre for Medium-Range Weather Forecasts (ECMWF) reanalysis data set (ERA5; Hersbach et al., 2020) for most atmosphere/ocean analysis. ERA5 currently extends from 1940–present at hourly temporal resolution. Potential intensity was calculated using the Bister and Emanuel (2002) method as implemented in the tcpyPI package from Gilford (2020, 2021). In keeping with NOAA's current 30-year climatology, we calculate all ERA5 anomalies relative to a 1991–2020 base period. Precipitation is calculated from the daily Global Precipitation Climatology Project data set (Huffman et al., 2001), which extends from October 1996–present and is available at 1° horizontal resolution.

2.3. Madden-Julian Oscillation Data

The MJO is a significant modulator of environmental conditions and TCs on sub-seasonal timescales (e.g., Chang et al., 2023; Hansen et al., 2020; Klotzbach & Oliver, 2015). We evaluate the state of the MJO using the methodology of Wheeler and Hendon (2004). This index estimates the phase and intensity of the MJO via 200 hPa zonal wind and 850 hPa zonal wind from the NCEP/NCAR Reanalysis (Kalnay et al., 1996) and interpolated outgoing longwave radiation from NOAA (Liebmann & Smith, 1996).

2.4. Moderate Resolution Imaging Spectroradiometer/Aerosol Optical Depth Data

The MODerate resolution Imaging Spectroradiometer (MODIS) instrument is mounted on both the Terra and Aqua satellites. MODIS measures reflected solar and emitted thermal radiation on 36 spectral channels which can then be used to assess various atmospheric properties including aerosol optical depth (AOD; Remer et al., 2005). Data from the Terra and Aqua satellites are available since February 2000 and July 2002, respectively. In this study, we analyze daily level-3 dark target and deep blue combined AOD at a 550 nm wavelength to assess potential impacts of Saharan dust on the hurricane season lull.

2.5. African Easterly Jet and Wave Diagnostics

It is well established that AEWs are common precursors ("seeds") to Atlantic TCs (Landsea, 1993; Nuñez Ocasio et al., 2024; Russell et al., 2017), and that these waves grow and propagate along the African easterly jet (Burpee, 1972; Nuñez Ocasio et al., 2021; Reed et al., 1977). To investigate the role of the African easterly jet and AEWs on the hurricane season lull, we assess the latitudinal location of the jet and the waves in ERA5 fields. We located the African easterly jet by finding the latitude of the maximum wind speed between 550 and 800 hPa of the 20°W–10°E zonally-averaged zonal wind field. We located AEWs through objective tracking based on Bercos-Hickey and Patricola (2021), where the tracking domain extends to 25°E to incorporate all known regions of AEW genesis (Nuñez Ocasio et al., 2021; Thorncroft et al., 2008). We note that Lawton et al. (2022) also uses ERA5 data for their AEW tracker.

3. Results

3.1. Northward Shift in AEW Tracks

Figure 1 displays the latitude of the African easterly jet maximum, the AEW track latitude and magnitude at 18°W and AOD averaged between 5.5° and 23.5°N, 57.5°–15.5°W. We focus on track latitude at 18°W since that is approximately where AEWs emerge from the west coast of Africa and is also typically where AEWs reach their maximum amplitude (Hamilton et al., 2017). While this study focuses on the reduction in TC activity from 20 August–23 September, we find that both the latitude of the African easterly jet maximum (Figure 1a) and AEW track latitude (Figure 1b, Figure S2 in Supporting Information S1) were generally well north of their average latitude from mid-July through early September. The African easterly jet averaged ∼3° poleward of its climatological position during August (Figure S3 in Supporting Information S1). The African easterly jet had a slightly weaker maximum amplitude but also stronger horizontal shear in 2024 relative to the 1991–2020 climatology (Figure S3 in Supporting Information S1), which is in agreement with Grist (2002)'s findings for wet years over

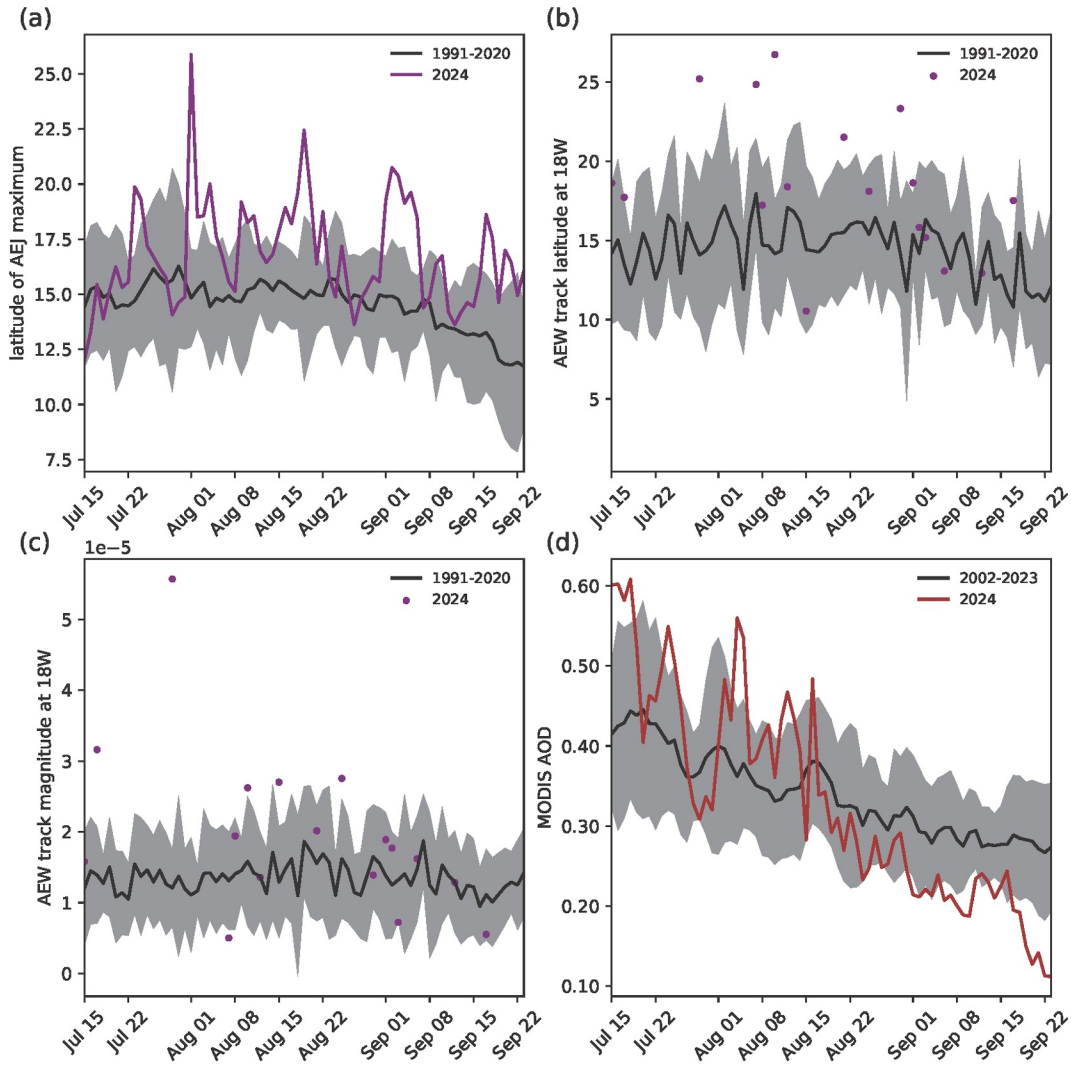

Figure 1. Western Africa and tropical Atlantic easterly jet maximum and African easterly wave (AEW) track latitude and amplitude, as well as Aerosol optical depth (AOD) from 15 July–23 September. (a) Latitude of African easterly jet maximum. (b) AEW track latitude at 18°W. The purple dots represent the individual AEW track latitudes at 18°W in 2024. (c) AEW track magnitude at 18°W as measured by 850 hPa curvature vorticity (s^{-1}). (d) AOD averaged from 5.5° to 23.5°N, 57.5°–15.5°W. The gray shading in panels (a), (b) and (c) represent a one standard deviation anomaly from the 1991–2020 average, while the shading in panel (d) represents a one standard deviation anomaly from the 2002–2023 average given the later start period of the MODerate resolution Imaging Spectroradiometer data set used to calculate AOD.

West Africa. The AEWs generally had a higher amplitude than average through late August, which agrees with observational and modeling studies that have shown that increased shear of the AEJ in wetter years leads to stronger waves (Bercos-Hickey et al., 2020, 2022; Grist, 2002). Higher AEW amplitude also typically favors their chances for TC formation (Figure 1c; Agudelo et al., 2011).

Precipitation across North Africa during August was also similar to what is typically observed with a strong West African monsoon (Figure S4 in Supporting Information S1), with enhanced precipitation across the Sahel and reduced precipitation in coastal African countries bordering the Gulf of Guinea (e.g., Landsea & Gray, 1992). However, precipitation was reduced closer to the coast of West Africa over Senegal, Guinea-Bissau and The Gambia, where anomalous low-level northerly winds associated with an anomalous low pressure near the west coast of Africa (Figure S5 in Supporting Information S1) may have advected dry air, suppressing precipitation. Enhanced precipitation did occur farther north in Mauritania and the Western Sahara, as expected given the observed August AEW tracks (Figure S2 in Supporting Information S1).

There was also anomalously high Saharan dust from mid-July through mid-August (Figure 1d). Bercos-Hickey et al. (2017) noted that increased dust could excite the northerly track of AEWs. These waves are less likely to become Atlantic TCs than their southerly track counterparts (Chen et al., 2008; Nuñez Ocasio et al., 2021), due both to climatologically less TC-favorable vertical wind shear and mid-level moisture conditions as well as an increased likelihood of recurvature over cooler SSTs in the eastern Atlantic. While these northerly track AEWs can form farther west in the basin (Chen et al., 2008), the aforementioned pronounced low-level northerly wind anomalies and associated dry air advection into the MDR (discussed in more detail in Section 3.4) likely squelched any chances for development farther west for these AEWs.

Dust decreased considerably around mid-August, yet AEWs predominately remained shifted northward during the last 2 weeks of August. This northward shift in the AEW emergence latitude resulted in few candidate AEWs for potential TC development. For example, on 25 August, the National Hurricane Center's Tropical Analysis and Forecast Branch was only tracking one anemic AEW near 45°W (https://www.nhc.noaa.gov/archive/text/TWDAT/2024/TWDAT.202408251738.txt). Two AEWs emerged north of 20°N during the lull, placing them at latitudes where SSTs were too cool in the eastern Atlantic to support robust TC development (e.g., <26.5°C; Gray, 1968) (Figures S6 and S7 in Supporting Information S1).

This lack of robust AEW candidates reduced the chances for TC formation when vertical wind shear conditions were quite favorable during the middle to latter part of August. As noted earlier, while AOD decreased around the middle of August, the African easterly jet and AEW tracks at 18°W remained well north of their average latitudes through the early part of September. The AEW track and latitude of the African easterly jet maximum shifted to more TC-conducive latitudes (e.g., closer to ∼15°) by early September; however, by this point, the MJO had become less favorable for TC development.

3.2. Atmospheric Stability and the Potential Intensity of TCs

The previous year (2023) exhibited an extremely busy peak Atlantic hurricane season, with 12 named storms forming between 20 August–23 September, tied with 2020 for the most Atlantic named storm formations on record between those two dates. Because 2024 was forecasted to be more active than 2023 and also had an extremely warm Atlantic, a comparison between the two seasons is instructive. While SSTs in the western and central tropical Atlantic were comparable to 2023, SSTs were considerably lower in the eastern tropical Atlantic in 2024 (Figures S6 and S7 in Supporting Information S1), especially north of ∼18°N which was where most AEWs emerged from the West African coast during the lull.

In addition to lower SSTs, 200 hPa temperatures were generally higher in 2024 than in 2023 across the eastern MDR during the lull period, resulting in a more stable atmosphere in 2024 (Figure S8 in Supporting Information S1). This anomalous upper-level warming was likely tied to the strong El Niño during the boreal winter of 2023–2024, as the upper troposphere warms substantially during El Niño events (Hogikyan et al., 2022). While El Niño dissipated during the spring of 2024, the upper-tropospheric temperature signal lags the SST signal by ∼3 months (Scherllin-Pirscher et al., 2012).

Here we examine how these higher upper-level temperatures impacted potential intensity (Bister & Emanuel, 2002), as upper-tropospheric temperatures are closely tied to the TC outflow temperature component of the potential intensity equation. We compare potential intensity during the 2024 Atlantic hurricane season lull with the 2023 Atlantic hurricane season during the same period (Figure 2). These comparisons are done using a z-score, which converts observed potential intensity anomalies to a normal distribution with a mean of 0 and a standard deviation of 1. Potential intensity in 2024 was notably reduced from 2023's values across the eastern Atlantic, especially north of 15°N, where the combination of lower SST and higher 200 hPa temperatures created a less conducive environment for the AEWs that emerged over the tropical Atlantic.

During the last week of the lull (Figure 2e), potential intensity increased in the eastern portion of the MDR, due in part to anomalous ocean warming associated with weak trade winds (not shown). These conditions created a more conducive thermodynamic environment for the flurry of late-season eastern MDR TCs (e.g., Joyce, Kirk, and Leslie). In addition, potential intensity anomalies also increased across the eastern Gulf, implying conducive atmospheric and oceanic conditions for what would become Hurricane Helene. These increasingly favorable potential intensity conditions likely helped end the 2024 Atlantic hurricane season lull with a flurry of TC activity as the MJO became more conducive (discussed in Section 3.3).

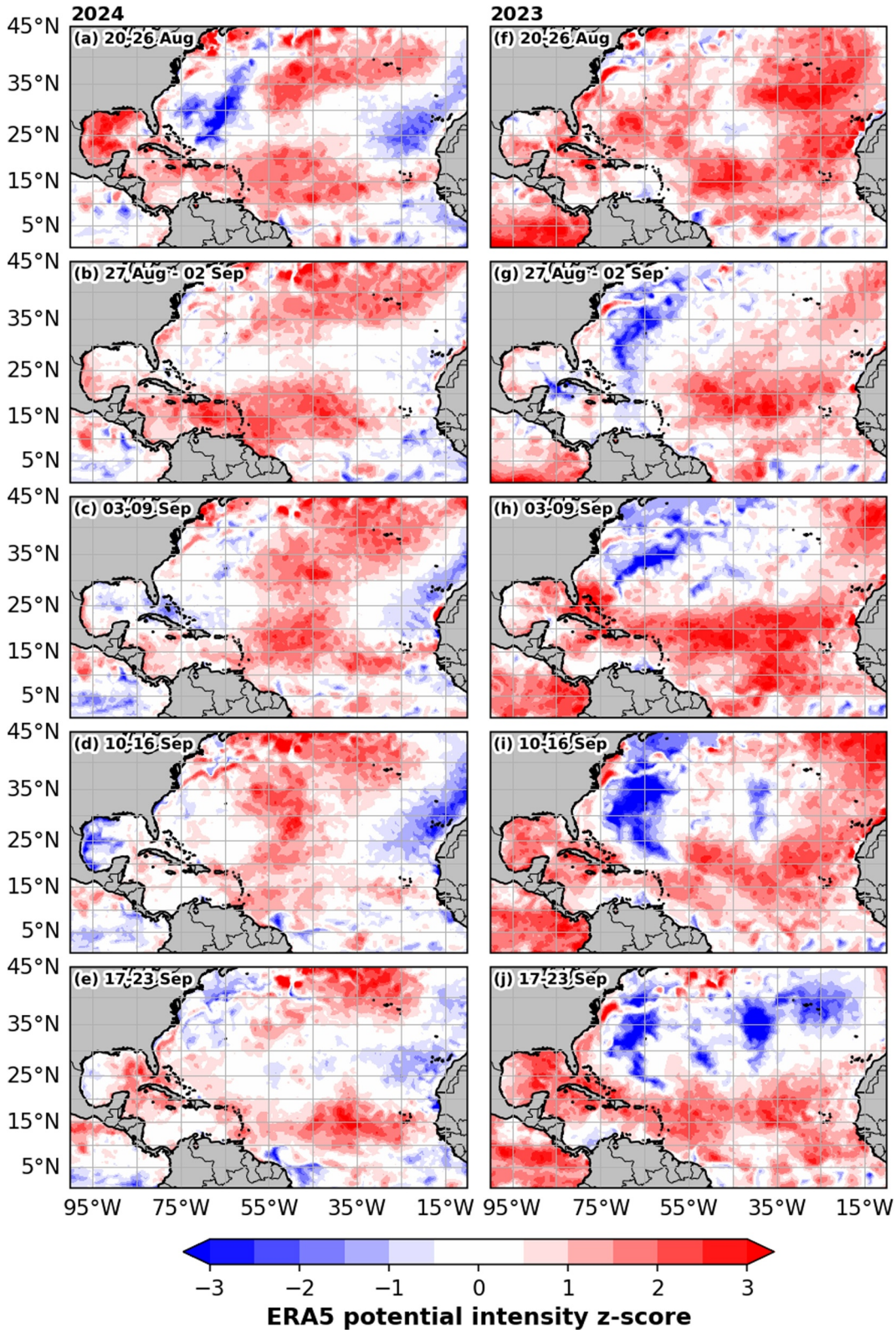

Figure 2. 2024 versus 2023 potential intensity across the Atlantic from 20 August–23 September. 2024 Potential intensity *z*-score anomalies during (a) 20–26 August, (b) 27 August–2 September, (c) 3–9 September, (d) 10–16 September, and (e) 17–23 September. (f–j) As in (a–e) but for 2023. Anomalies are calculated relative to a 1991–2020 base period.

3.3. Madden-Julian Oscillation Influence

The MJO was quite robust throughout most of the 2024 Atlantic hurricane season, with an amplitude >1 using the Wheeler and Hendon (2004) MJO index (Figure 3c). During most of August, the MJO was in phases typically considered conducive for Atlantic hurricane activity (e.g., phases 8–3) (e.g., Klotzbach & Oliver, 2015). These favorable subseasonal conditions, combined with the favorable seasonal conditions discussed previously, made the start of the lull around 20 August even more surprising. High amplitude MJO activity in phases 1–3 may have been one reason for the increased amplitude of mid-to-late August AEWs noted in Section 3.1 (e.g., Ventrice et al., 2011).

However, for the first 23 days of September, the MJO was in phases 4–7, which typically are associated with reduced Atlantic hurricane activity. Copious sinking motion occurred across most of the Atlantic during the lull (Figure 3a). This general sinking motion, combined with mid-level dryness associated with anomalous low-level northerly flow (see Section 3.4), combined to create non-conducive conditions for TC activity.

While vertical wind shear was generally lower than normal for most of August–October, there were two distinct packets of increased shear that propagated westward across the tropical Atlantic from late August to early September and mid to late September, respectively (Figure 3b, Figure S9 in Supporting Information S1). The westward propagation and phase speed of these shear anomalies (e.g., Wang et al., 2023) indicate that they could have been associated with westward-propagating equatorial Rossby wave activity. In addition, these anomalously high shear anomalies were generally co-located with weaker positive upper-level temperature anomalies (Figure S8 in Supporting Information S1), indicating that they were likely associated with a tropical upper tropospheric trough (Nieto Ferreira & Schubert, 1999) and enhanced anticyclonic wave breaking (e.g., Jones et al., 2020; Li et al., 2018). Tropical upper-tropospheric troughs typically have increased shear on their eastern flank (Li et al., 2018). These troughs also generally propagate west-southwestward with time, similar to what was observed with the two high shear packets (Nieto Ferreira & Schubert, 1999).

The enhanced shear and an associated increase in the low-level trade winds (Bucci & Alaka, 2025) associated with the first of these two shear pulses likely inhibited Francine's genesis until it entered a more conducive environment in the Bay of Campeche. Following the traverse of the second shear pulse across the Caribbean, the shear environment became highly conducive across almost the entire basin (Figure 3b). These two shear pulses also likely helped inhibit any potential TC development farther west in the basin during the lull.

Helene was named as a tropical storm on 24 September, coinciding with the day that the MJO emerged in Phase 8. Over the next couple of weeks, the MJO continued propagating eastward in favorable phases for Atlantic TC activity. The Atlantic produced five hurricanes and three major hurricanes between 24 September–11 October. During this time, vertical wind shear was well below normal across virtually the entire basin (Figure 3b, Figure S9 in Supporting Information S1). In addition, vertical motion was enhanced across the tropical Atlantic (Figure 3a) during the formation of Helene, Isaac, Joyce, Kirk, and Leslie.

3.4. Extratropical Influences

In addition to TC-unfavorable subseasonal conditions across the tropical Atlantic associated with the MJO, the extra-tropics likely contributed to the significant mid-level dryness that occurred near the climatological peak of the season (Figure 4). Anomalous northerly flow in the eastern and central Atlantic developed during late August and persisted through mid-September, advecting dry air into the eastern and central MDR (Figures 4b and 4c). A pronounced mid-level high pressure centered near Newfoundland and mid-level low pressure centered near Ireland were the likely synoptic-scale drivers of these anomalous northerly winds (Figures S10b–S10c in Supporting Information S1).

Mid-level dryness was noted by the National Hurricane Center as plaguing several systems during this time, including the National Hurricane Center's tropical weather outlook discussion on Invest 94L on 13 September (https://www.nhc.noaa.gov/archive/xgtwo/gtwo_archive.php?current_issuance=202409131436&basin=atl&fdays=7) as well as the forecast discussion for Tropical Storm Gordon on 13 September (https://www.nhc.noaa.gov/archive/2024/al07/al072024.discus.009.shtml). In particular, the Gordon discussion noted a “moisture-starved environment across the tropical Atlantic.”

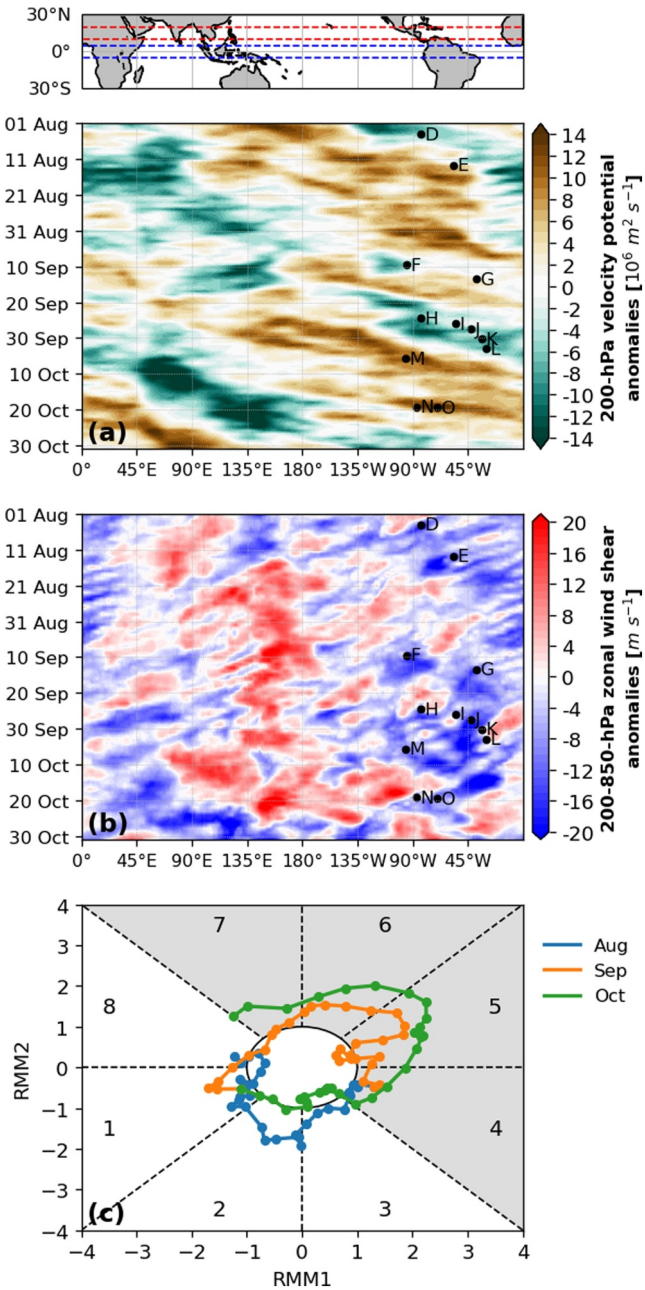

Figure 3. Tropical atmospheric variability during August–October 2024. (a) Hovmöller plot of 200 hPa velocity potential anomalies averaged from 5°S to 5°N. (b) Hovmöller plot of 200 hPa minus 850 hPa zonal wind anomalies averaged from 10° to 20°N. (c) Madden-Julian oscillation (MJO) propagation as measured by the Wheeler and Hendon (2004) index. Anomalies are calculated relative to a 1991–2020 base period. The schematic above panel a provides a geographical reference for the Hovmöller plot. The blue dashed lines denote the area-averaged region for panel (a), while the red dashed lines denote the area-averaged region for panel (b) The letters in panel b are the first letter of the particular storm name (e.g., "H" represents Helene). White shading in panel (c) highlights Atlantic TC-favorable MJO phases, while gray shading highlights Atlantic TC-unfavorable MJO phases.

By the 10–16 September period, the anomalous high near Newfoundland shifted eastward and then weakened substantially by the 17–23 September period (Figures S10d–S10e in Supporting Information S1). Associated with the shift in the large-scale steering flow pattern was a weakening of the trade winds and a moistening in the mid-levels across the MDR (Figures 4d and 4e). These more TC-favorable wind and moisture conditions likely supported the burst of activity that occurred immediately following the lull.

4. Conclusions

Though the 2024 Atlantic hurricane season ended up being hyperactive, the marked lull that occurred between 20 August–23 September was unexpected and highlighted how even with near record-high tropical Atlantic SSTs, cool neutral ENSO conditions, and a vigorous West African monsoon, TC activity can be markedly reduced by factors such as AEW positioning, anomalously high upper-level temperatures, TC-unfavorable subseasonal conditions associated with a convectively-suppressed MJO, and extratropical influences. The prolonged length of the lull was likely due to differing strengths of suppressive factors at different points during the lull. e.g., the start of the lull was likely due to a combination of AEWs emerging from Africa at latitudes that were too far north for TC development and anomalously high upper-level temperatures that suppressed chances for TC formation from other mechanisms due to increased stability and decreased potential intensity.

As the AEWs shifted to more conducive TC formation latitudes, the MJO became less conducive for Atlantic TC activity, with sinking motion occurring across the basin, along with brief periods of increased vertical wind shear. Anomalous northerly flow from a pronounced blocking pattern over the North Atlantic advected dry air into the eastern MDR, generating less TC-conducive thermodynamic conditions.

This study highlights that even well-anticipated seasonal SST conditions (e.g., near-record warm MDR and cool neutral/weak La Niña) can yield unanticipated outcomes. The 2024 Atlantic TC season provides a fascinating example of the complex interactions between large-scale thermodynamic conditions favorable to TCs, the African easterly jet and AEWs, interactions of various dynamically-driven large-scale phenomena, including the MJO and mid-latitude blocking, as well as chaotically-driven short-term weather events. As has been noted throughout this study, the lull was immediately followed by one of the busiest ends to an Atlantic hurricane season on record, including two major hurricane landfalls in Florida (Helene and Milton), resulting in more than 250 fatalities and >100 billion USD in damage (National Centers for Environmental Information, 2025). Though the final overall number of hurricanes and major hurricanes were aligned with the seasonal forecasts, the extremely busy beginning and end to the season and marked lull in the middle highlight just how unusual the season was.

While it seems somewhat unlikely to be able to anticipate this type of prolonged lull in a hyperactive season several months in advance, future work will investigate improved prediction of lulls several weeks prior to their onset. For example, while vertical wind shear and SST conditions were extremely conducive in July, dust AOD in the tropical Atlantic was also above normal. As noted earlier, increased dust in the eastern tropical Atlantic can excite the

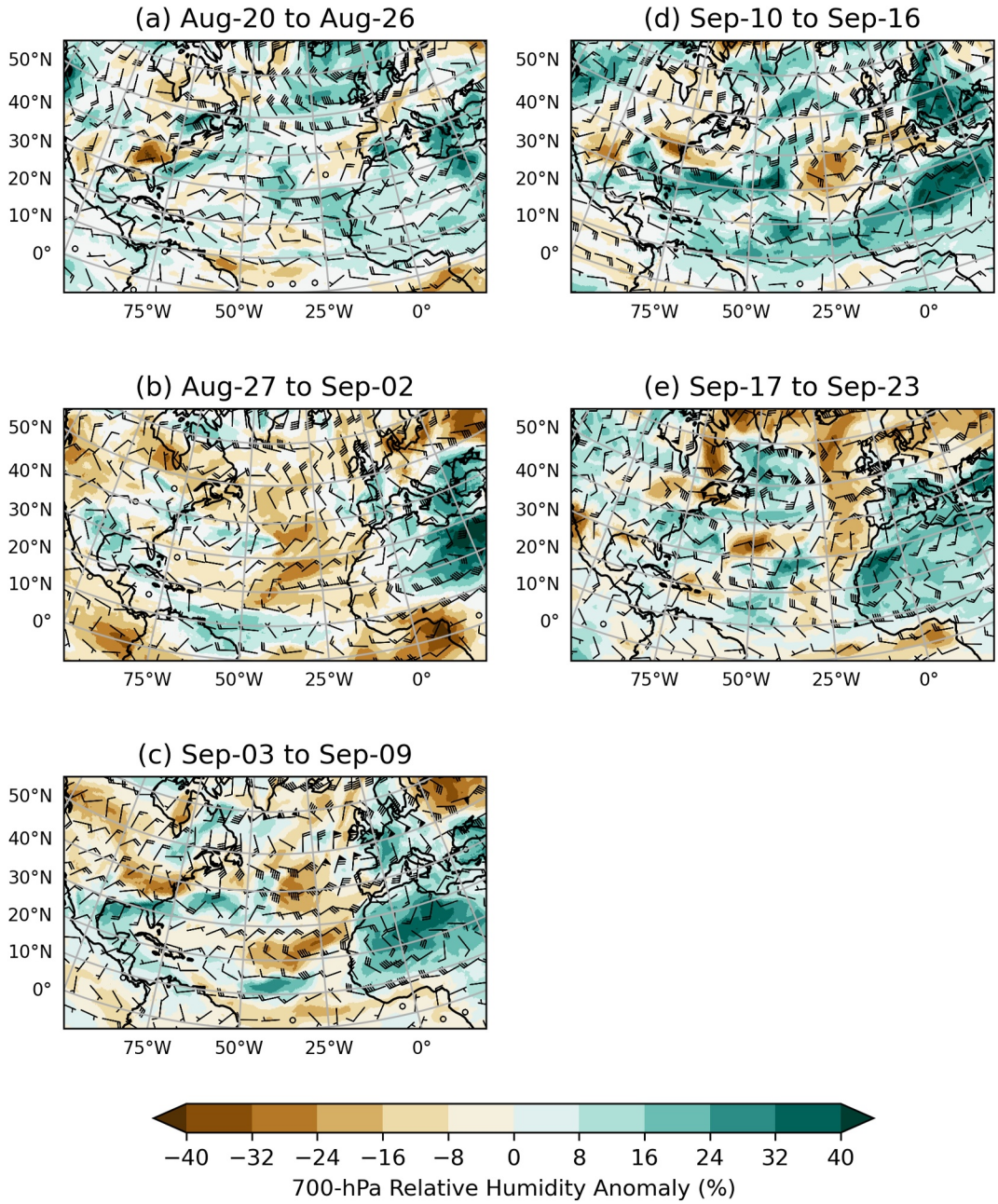

Figure 4. Anomalous 700-hPa relative humidity (shading) and 700-hPa winds (vectors). (a) 20–26 August anomalies. (b) 27 August–2 September anomalies. (c) 3–9 September anomalies. (d) 10–16 September anomalies. (e) 17–23 September anomalies. Full wind vector barbs represent 2 m s^{-1} anomalies, while flags represent 10 m s^{-1} anomalies. Anomalies are calculated relative to a 1991–2020 base period.

northerly track of AEWs. In future seasons, we suggest that groups issuing seasonal forecasts consider dust AOD in July to evaluate whether they deviate from their typical inverse relationship with Atlantic SSTs and vertical wind shear (Xian et al., 2020). In addition, given continued upper-level warming associated with climate change, seasonal TC forecasts may need to explore upper-level temperatures or potential intensity metrics as alternative thermodynamic predictors to SSTs.

Data Availability Statement

Atlantic TC activity from 1851 to 2024 were taken from the HURDAT2 data set (National Hurricane Center, 2025). Most environmental parameter data were taken from hourly ECMWF reanalysis pressure level (Hersbach et al., 2023a) and hourly ECMWF reanalysis surface level (Hersbach et al., 2023b) data. Daily Global Precipitation Climatology Project data were downloaded from Adler et al. (2017).

Acknowledgments

We would like to acknowledge helpful comments from Chris Landsea and an anonymous reviewer that significantly improved the manuscript. P. Klotzbach, M. Bell, and L. Silvers acknowledge funding from the G. Unger Vetlesen Foundation, National Science Foundation (NSF) Award Number AGS-2331202 and from Gallagher Re through the Gallagher Research Centre Global Tropical Cyclone Consortium. C. Patricola acknowledges support from the US Department of Energy, Office of Science, Office of Biological and Environmental Research, Earth and Environmental Systems Modeling (EESM) Program, Early Career Research Program Award Number DE-SC0021109. E. Bercos-Hickey acknowledges support from the U.S. Department of Energy, Office of Science, Office of Biological and Environmental Research, Climate and Environmental Sciences Division, Regional & Global Model Analysis Program, under Award Number DE-AC02-05CH11231. Schreck was supported by NOAA through the Cooperative Institute for Satellite Earth System Studies under Cooperative Agreement NA19NES5320002. D. Chavas was supported by NSF Award Number 1945113. K. Wood was supported by NSF Award Number AGS-2403487. We dedicate this paper to our deceased coauthor Ethan Gibney who made many important contributions to the field of tropical meteorology.

References

Adler, R., Wang, J.-J., Sapiano, M., Huffman, G., Bolvin, D., & Nelkin, E., & NOAA CDR Program. (2017). Global precipitation climatology project (GPCP) climate data record (CDR), version 1.3 [Dataset]. *NOAA National Centers for Environmental Information*. https://doi.org/10.7289/V5RX998Z

Agudelo, P. A., Hoyos, C. D., Curry, J. A., & Webster, P. J. (2011). Probabilistic discrimination between large-scale environments of intensifying and decaying African Easterly Waves. *Climate Dynamics*, *36*(7–8), 1379–1401. https://doi.org/10.1007/s00382-010-0851-x

Bell, G. D., Halpert, M. S., Schnell, R. C., Higgins, R. W., Lawrimore, J., Kousky, V. E., et al. (2000). Climate assessment for 1999. *Bulletin of the American Meteorological Society*, *81*(6), S1–S50. https://doi.org/10.1175/1520-0477(2000)81[s1:CAF]2.0.CO;2

Bercos-Hickey, E., Nathan, T. R., & Chen, S. (2020). On the relationship between the African easterly jet, Saharan mineral dust aerosols, and West African precipitation. *Journal of Climate*, *33*(9), 3533–3546. https://doi.org/10.1175/JCLI-D-18-0661.1

Bercos-Hickey, E., Nathan, T. R., & Chen, S. (2022). Effects of Saharan dust aerosols and West African precipitation on the energetics of African easterly waves. *Journal of the Atmospheric Sciences*, *79*(7), 1911–1926. https://doi.org/10.1175/JAS-D-21-0157.1

Bercos-Hickey, E., Nathan, T. R., & Chen, S.-H. (2017). Saharan dust and the African easterly jet–African easterly wave system: Structure, location and energetics. *Quarterly Journal of the Royal Meteorological Society*, *143*(708), 2797–2808. https://doi.org/10.1002/qj.3128

Bercos-Hickey, E., & Patricola, C. M. (2021). Anthropogenic influences on the African easterly jet–African easterly wave system. *Climate Dynamics*, *57*(9), 2779–2792. https://doi.org/10.1007/s00382-021-05838-1

Bister, M., & Emanuel, K. A. (2002). Low frequency variability of tropical cyclone potential intensity 1. Interannual to interdecadal variability. *Journal of Geophysical Research*, *107*(D24), 4801. https://doi.org/10.1029/2001JD000776

Bucci, L., & Alaka, L. (2025). *Tropical cyclone report: Hurricane Francine (AL062024). 9–12 September 2024*. National Hurricane Center. Retrieved from https://www.nhc.noaa.gov/data/tcr/AL062024_Francine.pdf

Burpee, R. W. (1972). The origin and structure of easterly waves in the lower troposphere of North Africa. *Journal of the Atmospheric Sciences*, *29*(1), 77–90. https://doi.org/10.1175/1520-0469(1972)029<0077:TOASOE>2.0.CO;2

Chang, C., Lubis, S. W., Balaguru, K., Leung, L. R., Hagos, S. M., & Klotzbach, P. J. (2023). An extratropical pathway for the Madden–Julian oscillation's influence on North Atlantic tropical cyclones. *Journal of Climate*, *36*(24), 8539–8559. https://doi.org/10.1175/JCLI-D-23-0251.1

Chen, T.-C., Wang, S.-Y., & Clark, A. J. (2008). North Atlantic hurricanes contributed by African easterly waves north and south of the African easterly jet. *Journal of Climate*, *21*(24), 6767–6776. https://doi.org/10.1175/2008jcli2523.1

Delgado, S., Landsea, C. W., & Willoughby, H. (2018). Reanalysis of the 1954–63 Atlantic hurricane seasons. *Journal of Climate*, *31*(11), 4177–4192. https://doi.org/10.1175/JCLI-D-15-0537.1

Gilford, D. M. (2020). pyPI: Potential intensity calculations in Python, pyPI v1.3. *Zenodo*. https://doi.org/10.5281/zenodo.3985975

Gilford, D. M. (2021). pyPI: Tropical cyclone potential intensity calculations in Python. *Geoscientific Model Development*, *14*(5), 2351–2369. https://doi.org/10.5194/gmd-14-2351-2021

Gray, W. M. (1968). Global view of the origin of tropical disturbances and storms. *Monthly Weather Review*, *96*(10), 669–700. https://doi.org/10.1175/1520-0493(1968)096<0669:GVOTOO>2.0.CO;2

Gray, W. M. (1984). Atlantic seasonal hurricane frequency. Part I: El Niño and 30 mb Quasi-biennial oscillation influences. *Monthly Weather Review*, *112*(9), 1649–1668. https://doi.org/10.1175/1520-0493(1984)112<1649:ASHFPI>2.0.CO;2

Grist, J. P. (2002). Easterly waves over Africa. Part I: The seasonal cycle and contrasts between wet and dry years. *Monthly Weather Review*, *130*(2), 197–211. https://doi.org/10.1175/1520-0493(2002)130<0197:EWOAPI>2.0.CO;2

Hagen, A. B., & Landsea, C. W. (2012). On the classification of extreme Atlantic hurricanes utilizing mid-twentieth-century monitoring capabilities. *Journal of Climate*, *25*(13), 4461–4475. https://doi.org/10.1175/JCLI-D-11-00420.1

Hamilton, H. L., Young, G. S., Evans, J. L., Fuentes, J. D., & Núñez Ocasio, K. M. (2017). The relationship between the Guinea Highlands and the West African offshore rainfall maximum. *Geophysical Research Letters*, *44*(2), 1158–1166. https://doi.org/10.1002/2016GL071170

Hansen, K. A., Majumdar, S. J., & Kirtman, B. P. (2020). Identifying subseasonal variability relevant to Atlantic tropical cyclone activity. *Weather and Forecasting*, *35*(5), 2001–2024. https://doi.org/10.1175/WAF-D-19-0260.1

Hersbach, H., Bell, B., Berrisford, P., Biavati, G., Horanyi, A., Munoz Sabater, J., et al. (2023a). ERA5 hourly data on pressure levels from 1940 to present [Dataset]. *Copernicus Climate Change Service (C3S) Climate Data Store (CDS)*. https://doi.org/10.24381/cds.bd0915c6

Hersbach, H., Bell, B., Berrisford, P., Biavati, G., Horanyi, A., Munoz Sabater, J., et al. (2023b). ERA5 hourly data on surface levels from 1940 to present [Dataset]. *Copernicus Climate Change Service (C3S) Climate Data Store (CDS)*. https://doi.org/10.24381/cds.adbb2d47

Hersbach, H., Bell, B., Berrisford, P., Hirahara, S., Horanyi, A., Munoz-Sabater, J., et al. (2020). The ERA5 global reanalysis. *Quarterly Journal of the Royal Meteorological Society*, *146*(730), 1999–2049. https://doi.org/10.1002/qj.3803

Hogikyan, A., Resplandy, L., & Fuegliaster, S. (2022). Cause of the intense tropics-wide tropospheric warming response to El Niño. *Journal of Climate*, *35*(10), 2933–2944. https://doi.org/10.1175/JCLI-D-21-0728.1

Huffman, G. J., Adler, R. F., Morrissey, M. M., Bolvin, D. T., Curtis, S., Joyce, R., et al. (2001). Global precipitation at one-degree daily resolution from multisatellite observations. *Journal of Hydrometeorology*, *2*(1), 36–50. https://doi.org/10.1175/1525-7541(2001)002<0036:GPAODD>2.0.CO;2

Jones, J., Bell, M. M., & Klotzbach, P. J. (2020). Tropical and subtropical North Atlantic vertical wind shear and seasonal tropical cyclone variability. *Journal of Climate*, *33*(13), 5413–5446. https://doi.org/10.1175/JCLI-D-19-0474.1

Kalnay, E., Kanamitsu, M., Kistler, R., Collins, W., Deaven, D., Gandin, L., et al. (1996). The NCEP/NCAR 40-year reanalysis project. *Bulletin of the American Meteorological Society*, *77*(3), 437–472. https://doi.org/10.1175/1520-0477(1996)077<0437:tnyrp>2.0.co;2

Keim, B. D., Hamilton, L. C., Brown, V. M., Klotzbach, P. J., Lewis, A. B., & Thompson, D. T. (2024). Lengthening Atlantic hurricane seasons with earlier storm formation dates including implications from 2020. *Journal of Climate*, *37*(24), 6699–6712. https://doi.org/10.1175/JCLI-D-23-0507.1

Klotzbach, P. J., & Oliver, E. C. J. (2015). Modulation of Atlantic basin tropical cyclone activity by the Madden–Julian oscillation (MJO) from 1905 to 2011. *Journal of Climate*, *28*(1), 204–217. https://doi.org/10.1175/JCLI-D-14-00509.1

Klotzbach, P. J., Wood, K. M., Bell, M. M., Blake, E. S., Bowen, S. G., Caron, L., et al. (2022). A hyperactive end to the Atlantic hurricane season October–November 2020. *Bulletin of the American Meteorological Society*, *103*(1), E110–E128. https://doi.org/10.1175/BAMS-D-20-0312.1

Landsea, C. W. (1993). A climatology of intense (or major) Atlantic hurricanes. *Monthly Weather Review*, *121*(6), 1703–1713. https://doi.org/10.1175/1520-0493(1993)121<1703:acoima>2.0.co;2

Landsea, C. W., & Franklin, J. L. (2013). Atlantic hurricane database uncertainty and presentation of a new database format. *Monthly Weather Review*, *141*(10), 3576–3592. https://doi.org/10.1175/MWR-D-12-00254.1

Landsea, C. W., & Gray, W. M. (1992). The strong association between western Sahelian monsoon rainfall and intense Atlantic hurricanes. *Journal of Climate*, *5*(5), 435–453. https://doi.org/10.1175/1520-0442(1992)005<0435:TSABWS>2.0.CO;2

Lawton, Q. A., Majumdar, S. J., Dotterer, K., Thorncroft, C., & Schreck, C. J., III. (2022). The influence of convectively coupled Kelvin waves on African easterly waves in a wave-following framework. *Monthly Weather Review*, *150*(8), 2055–2072. https://doi.org/10.1175/MWR-D-21-0321.1

Li, W., Wang, Z., Zhang, G., Peng, M. S., Benjamin, S. G., & Zhao, M. (2018). Subseasonal variability of Rossby wave breaking and impacts on tropical cyclones during the North Atlantic warm season. *Journal of Climate*, *31*(23), 9679–9695. https://doi.org/10.1175/JCLI-D-17-0880.1

Liebmann, B., & Smith, C. A. (1996). Description of a complete (interpolated) outgoing longwave radiation dataset. *Bulletin of the American Meteorological Society*, *77*(6), 1275–1277. http://www.jstor.org/stable/26233278

National Hurricane Center. (2025). The revised Atlantic hurricane database (HURDAT2) [Dataset]. *National Oceanic and Atmospheric Administration*. Retrieved from https://www.aoml.noaa.gov/hrd/hurdat/hurdat2.html

Nieto Ferreira, R., & Schubert, W. H. (1999). The role of tropical cyclones in the formation of tropical upper-tropospheric troughs. *Journal of the Atmospheric Sciences*, *56*(16), 2891–2907. https://doi.org/10.1175/1520-0469(1999)056<2891:trotci>2.0.co;2

NOAA National Centers for Environmental Information (NCEI). (2025). U.S. Billion-dollar weather and climate disasters. https://doi.org/10.25921/stkw-7w73

Nuñez Ocasio, K., Brammar, A., Evans, J. L., Young, G. S., & Moon, Z. L. (2021). Favorable monsoon environment over eastern Africa for subsequent tropical cyclogenesis of African easterly waves. *Journal of the Atmospheric Sciences*, *78*(9), 2911–2925. https://doi.org/10.1175/JAS-D-20-0339.1

Núñez Ocasio, K. M., Davis, C. A., Moon, Z. L., & Lawton, Q. A. (2024). Moisture dependence of an African easterly wave within the West African monsoon system. *Journal of Advances in Modeling Earth Systems*, *16*(6), e2023MS004070. https://doi.org/10.1029/2023MS004070

Patricola, C. M., Saravanan, R., & Chang, P. (2014). The impact of the El Niño–Southern oscillation and Atlantic meridional mode on seasonal Atlantic tropical cyclone activity. *Journal of Climate*, *27*(14), 5311–5328. https://doi.org/10.1175/JCLI-D-13-00687.1

Reed, R. J., Norquist, D. C., & Recker, E. E. (1977). The structure and properties of African wave disturbances as observed during Phase III of GATE. *Monthly Weather Review*, *105*(3), 317–333. https://doi.org/10.1175/1520-0493(1977)105<0317:TSAPOA>2.0.CO;2

Remer, L. A., Kaufman, Y. J., Tanré, D., Mattoo, S., Chu, D. A., Martins, J. V., et al. (2005). The MODIS Aerosol Algorithm, products, and validation. *Journal of the Atmospheric Sciences*, *62*(4), 947–973. https://doi.org/10.1175/JAS4385.1

Russell, J. O., Aiyyer, A., White, J. D., & Hannah, W. (2017). Revisiting the connection between African easterly waves and Atlantic tropical cyclogenesis. *Geophysical Research Letters*, *44*(1), 587–595. https://doi.org/10.1002/2016GL071236

Scherllin-Pirscher, B., Deser, C., Ho, S.-P., Chou, C., Randel, W., & Kuo, Y.-H. (2012). The vertical and spatial structure of ENSO in the upper troposphere and lower stratosphere from GPS radio occultation measurements. *Geophysical Research Letters*, *39*(20), L20801. https://doi.org/10.1029/2012GL053071

Thorncroft, C. D., Hall, N. M. J., & Kiladis, G. N. (2008). Three-dimensional structure and dynamics of African easterly waves. Part III: Genesis. *Journal of the Atmospheric Sciences*, *65*(11), 3596–3607. https://doi.org/10.1175/2008JAS2575.1

Ventrice, M. J., Thorncroft, C. D., & Roundy, P. E. (2011). The Madden–Julian Oscillation's influence on African easterly waves and downstream tropical cyclogenesis. *Monthly Weather Review*, *139*(9), 2704–2722. https://doi.org/10.1175/MWR-D-10-05028.1

Wang, J., Yang, R., & Cao, J. (2023). Interdecadal variation of atmospheric equatorial Rossby waves during boreal summer. *Atmospheric Research*, *290*, 106782. https://doi.org/10.1016/j.atmosres.2023.106782

Wheeler, M. C., & Hendon, H. H. (2004). An all-season real-time multivariate MJO index: Development of an index for monitoring and prediction. *Monthly Weather Review*, *132*(8), 1917–1932. https://doi.org/10.1175/1520-0493(2004)132<1917:AARMMI>2.0.CO;2

Xian, P., Klotzbach, P. J., Dunion, J. P., Janiga, M. A., Reid, J. S., Colarco, P. R., & Kipling, Z. (2020). Revisiting the relationship between Atlantic dust and tropical cyclone activity using aerosol optical depth reanalyses: 2003–2018. *Atmospheric Chemistry and Physics*, *20*(23), 15357–15378. https://doi.org/10.5194/acp-20-15357-2020